RSC Advances

PAPER

View Article Online
View Journal | View Issue

Cite this: *RSC Adv.*, 2018, **8**, 36239

Synthesis of antimicrobial AlOOH–Ag composite nanostructures by water oxidation of bimetallic Al–Ag nanoparticles

Lozhkomoev Aleksandr,[a] Pervikov Alexander,[a] Bakina Olga,[a]* Kazantsev Sergey[a] and Gotman Irena[b]

The facile one-step synthesis of AlOOH–Ag nanocomposite has been performed. Bimetallic Al–Ag nanoparticles prepared by electrical explosion of Al and Ag wires were used as a precursor. AlAg nanoparticles consisted of a supersaturated Al–6 at% Ag solid solution and Ag-rich Guinier–Preston zone several nanometer in diameter that were not detected by XRD due to their extremely small size and peculiarities of their crystal structure. An environmentally friendly process of water oxidation at 60 C was used to convert Al–Ag nanoparticles into AlOOH–Ag nanocomposites. In the course of oxidation, chemical dealloying of Al–Ag solid solution took place yielding porous agglomerates with inclusions of very fine 5–30 nm Ag nanoparticles. The agglomerates consisted of 2–5 nm thick crumpled nanosheets of boehmite 200 nm in size. The synthesized AlOOH–Ag nanocomposites possessed high antibacterial activity against both Gram-negative and Gram-positive microorganisms as indicated by the time-kill assay. The presented results open up new processing possibilities of metal-oxide composite nanostructures with attractive properties that can be used in catalysis, water purification and biomedical applications.

Received 16th May 2018
Accepted 6th October 2018

DOI: 10.1039/c8ra04173c

rsc.li/rsc-advances

Introduction

The unique features of composite nanoparticles that combine or even enhance the favorable intrinsic properties of the constituents on the nanoscale, make them attractive candidate materials for many important scientific and industrial applications, including but not limited to water purification,[1] catalysis,[2] and biomedicine.[3,4] The design and development of new composite nanoparticles with unusual structures, different morphologies, or special components can significantly broaden the application spectrum of these materials. One of the promising types of nanoscale materials are composites based on aluminum oxide and hydroxide nanosheets, due to their thermal stability, low cost, well-developed porosity, high absorption capacity, controllable surface concentration of acidic and basic centers and low toxicity.[5–7] Specifically, novel anticancer and antimicrobial agents can be developed by using nanoscale AlOOH as a platform for the attachment of bactericidal metals or metals that affect cellular functions.

The authors of[8] prepared hierarchical copper- and zinc- buds dressing γ-AlOOH mesostrands with randomly wrinkled morphology by reacting aluminum chloride with Cu- or Zn chloride dihydrate. The mesostrands markedly enhanced cellular uptake of a model cancer antigen in antigen presenting cells and were considered as valuable immunoadjuvants for cancer immunotherapy. In[9] gold nanoparticle doped mesoporous boehmite films were synthesized by hot hydrolysis of aluminumtri-*sec*-butoxide, admixing of $HAuCl_4$ to the obtained AlOOH-sol and finally film deposition on glass slides. The films obtained exhibited excellent catalytic activities in both the organic and inorganic electron transfer reactions in aqueous solutions with high rate constant values.

Silver and silver compounds have a well-documented wide spectrum antimicrobial activity that is greatly enhanced when silver is used in the form of nanoparticles. The applications of Ag nanoparticles range from water purification to paints, coatings on textile fabrics, food packaging and medical applications.[10–12] The authors of[13] developed an innovative thermal decomposition–reduction method of producing silver nanoparticles 22 to 60 nm in size incorporated into an aluminum nano-oxide substrate. Such Al_2O_3–Ag nanopowders exhibited bactericidal and fungicidal activities against several bacteria and fungus strains due positive zeta-potential of Al_2O_3. Al_2O_3 powder with 15–20 nm Ag nanoparticles evenly distributed on the surface prepared by introducing Al_2O_3 into silver nitrate aqueous solution were also reported to demonstrate strong bactericidal action against *E. coli*.[14,15] Most preparation methods of metal-aluminum oxide-based composites are based either on co-deposition of the oxide and metal from salts, or on surface modification of the oxide by metal nanoparticles. Water oxidation of bimetallic nanoparticles is an attractive alternative approach to the synthesis such nanocomposites. It has been

[a]*Institute of Strength Physics and Materials Science of Siberian Branch of Russian Academy of Sciences, Tomsk, Russia. E-mail: ovbakina@ispms.tsc.ru*
[b]*Department of Mechanical Engineering, ORT Braude College, Karmiel, Israel*

reported earlier that the reaction of bimetallic Al–Cu nanoparticles with water leads to the formation of porous nanocomposites comprised of crumpled sheets of AlOOH (pseudoboehmite) and nanosized inclusions of copper and Cu–Al intermetallics.[16] Similarly, Al–Zn bimetallic nanoparticles react with water yielding an AlOOH–ZnO–Zn porous nanocomposite.[17] Both AlOOH–Cu and AlOOH–Zn nanocomposites were reported to have pronounced antimicrobial activity.

In the present paper, the process of water oxidation of bimetallic Ag–Al nanoparticles was investigated and the antibacterial activity of the synthesized AlOOH–Ag nanocomposites was assessed.

Results and discussion

Characterization of Al–Ag bimetallic nanoparticles

In present work we obtained Ag–Al nanoparticles by electric explosion of two aluminum and silver wires for the first time. This method allows to produce nanopowders with high productivity in the amount of 50 g h^{-1}. Ag–Al nanoparticles are air-stable, but they are easily oxidized by water when heated to 60 °C. Fig. 1 shows representative TEM images and EDS map of Ag–Al bimetallic nanoparticles. It can be seen that the particles are spherical in shape with a fairly uniform distribution of Al and Ag. The atomic ratio of the two metals in the nanoparticles as measured by EDS (83 at% Al–17 at% Ag) is close to their ratio in the starting wires.

XRD pattern of Ag–Al nanoparticles is presented in Fig. 2a. The pattern shows that the structure is a single FCC phase, *i.e.* a solid solution of Ag in Al. A similar XRD pattern was reported in[20] for a rapidly solidified 85Al–15Ag alloy. The calculated lattice parameter is 0.4049 nm which corresponds to pure Al. It has been reported, however, that the lattice spacing of Al based solution remains practically unchanged up to 6 at% Ag.[21] It is therefore assumed that our electrically exploded Ag–Al nanoparticles

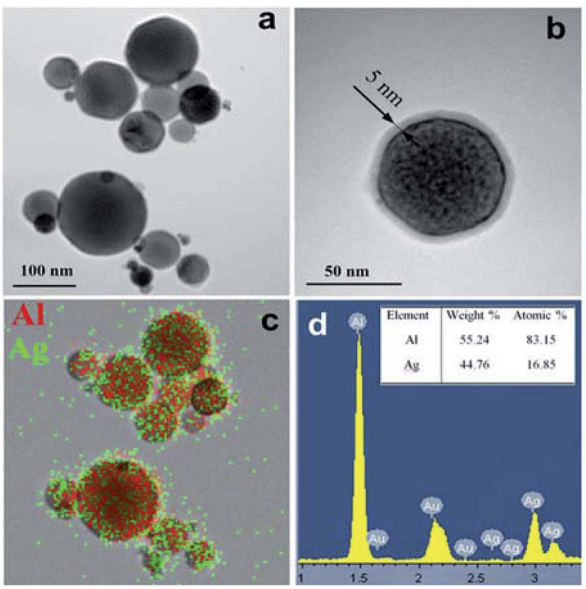

Fig. 1 TEM images (a and b), EDS map (c) and quantitative EDS analysis (d) of bimetallic Ag–Al nanoparticles.

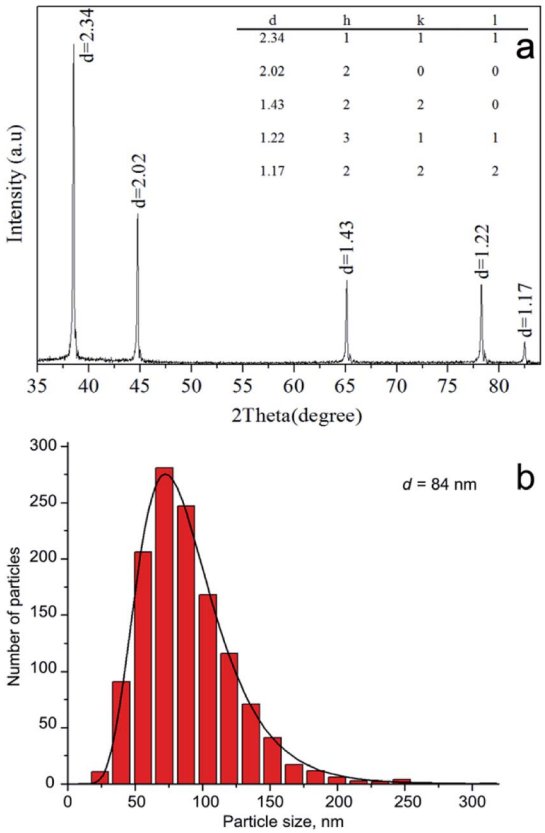

Fig. 2 XRD pattern of Al–Ag bimetallic nanoparticles (a) and their size distribution (b).

consist of a supersaturated Al–6 at% Ag solid solution and Ag-rich GP zones several nanometer in diameter that are not detected by XRD due to their extremely small size and peculiarities of their crystal structure.[22] Such Ag clusters of about 1 nm in radius were observed, for example, by high resolution TEM in an Al–Ag alloy quenched from 560 °C.[23] In our case, the formation of a supersaturated solid solution with Ag-rich GP zones may be explained by the very rapid cooling of the Al–Ag liquid alloy formed at the high electric explosion temperature.[24] The compositionally inhomogeneous structure of the electrically exploded Ag–Al nanoparticles is confirmed by contrast fluctuations observed in the TEM images in Fig. 1. The crystallite size of the Al–Ag solid solution is approximately 70 nm. At the same time, the Ag–Al bimetallic nanoparticles have a log normal size distribution with the maximum at 84 nm (Fig. 2b). The ratio of the average particle size and the crystallite size is similar to the one reported for the electrically exploded copper and cobalt nanoparticles.[24,25] The smaller crystallite size compared to the particle size may be due to the presence of a roentgenographically amorphous surface oxide layer (Fig. 1b), as well as to the polycrystalline structure of some Ag–Al nanoparticles.

Water oxidation of Al–Ag bimetallic nanoparticles

The process of water oxidation of bimetallic Al–Ag nanoparticles was monitored by pH evolution in the course of reaction. This allowed us to establish the exact time of reaction completion and

thus to obtain the final product avoiding the unnecessary aging in the mother liquor. The kinetic curves of pH and temperature evolution of the reaction medium upon heating of a 1 wt% suspension of Al–Ag nanoparticles are presented in Fig. 3. The pH curve is similar to the one obtained for the water oxidation of Al nanopowder.[19] A slow pH increase in the beginning of reaction (due to the heating of the reaction medium) is followed by the faster pH increase caused by the intensive hydration of the surface oxide film. The heating of the reaction medium to 55 °C is accompanied by the pH drop and a steep temperature rise due to the exothermic heat released by the reaction of aluminum with water. After one minute, the pH starts to rise again until at levels off when the reaction is complete.

Characterization of AlOOH–Al composite nanoparticles

Fig. 4 shows representative TEM images and EDS maps of water oxidation products of Ag–Al nanoparticles 50 minutes after the reaction start.

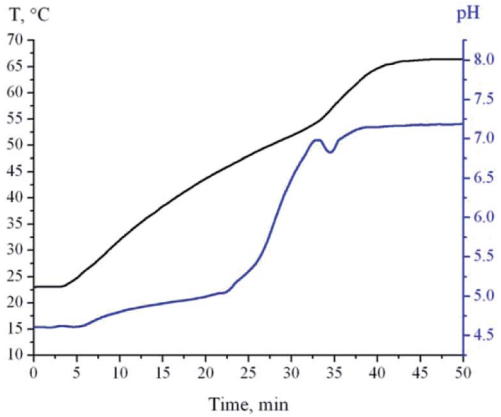

Fig. 3 pH and temperature of reaction medium *versus* immersion time of Al–Ag nanoparticles in water.

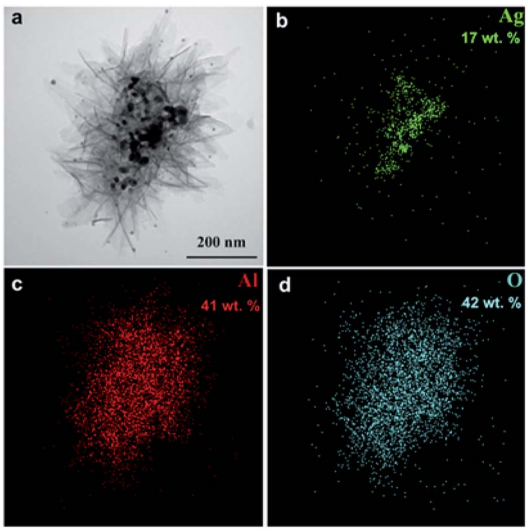

Fig. 4 TEM image of the oxidation product of Al–Ag nanoparticles (a) and the corresponding EDS maps of Ag (b), Al (c) and O (d).

The material synthesized consists of nanocomposite agglomerates up to 2 μm in size that are comprised of crumpled 2–5 nm thick nanosheets 200 nm in size and numerous near-spherical nanoparticles 3 to 30 nm in diameter (Fig. 5a).

According to XRD analysis (Fig. 5b), the material is composed of AlOOH (boehmite) and pure silver (lattice parameter 0.4086 nm). For Ag, the average size of coherent scattering domain is 14 nm, quite in agreement with the TEM data. A reliable XRD determination of coherent scattering domain size is complicated by substantial peak broadening caused by the very small crystallite size as well as by possible crystal lattice microstrain. Thus, the final product of water oxidation of bimetallic Ag–Al nanoparticles are AlOOH–Ag nanocomposite particles based on crumpled nanosheets of boehmite with inclusions of very fine silver nanoparticles.

The FTIR spectra of AlOOH–Ag nanocomposite is shown in Fig. 6a. The strong, broad band at 3295 cm^{-1} is assigned to the ν_{as} (Al)O–H and ν_{s} (Al)O–H stretching vibrations.[26]

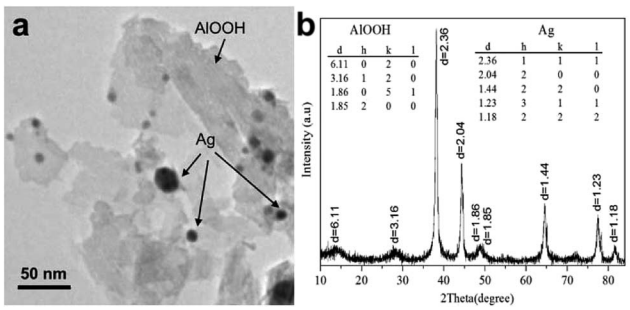

Fig. 5 High-resolution TEM-image (a) and XRD pattern (b) of the oxidation product of Al–Ag nanoparticles.

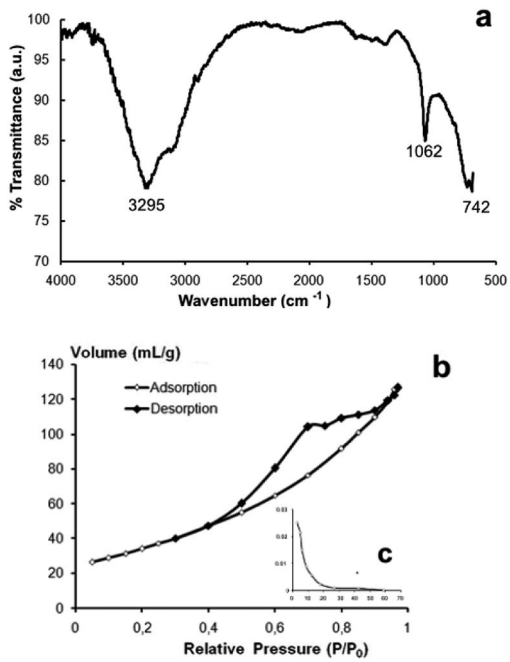

Fig. 6 FT-IR spectra (a), nitrogen adsorption–desorption isotherm (b) and pore size distribution (c) of AlOOH–Ag nanocomposite.

The band at 1062 cm^{-1} is assigned to the δ_s Al–O–H mode of γ-AlOOH. The strong band at 742 cm^{-1} is ascribed to the vibration mode of AlO_6. Based on the analysis of the adsorption–desorption isotherms of AlOOH–Ag nanocomposite, they can be referred to as mesoporous materials (average pore size = 4–10 nm). The isotherm of type IV (IUPAC) shows pronounced hysteresis loop relative pressures in the range of 0.4–0.9, which characterize mesopores (Fig. 6b). The specific surface area of the obtained nanocomposite is 183 ± 9 m^2 g^{-1} and its zeta potential in water at 25 °C is 25.4 ± 0.3 mV. The process of formation of Ag nanoparticles is in a way similar to the chemical dealloying method as described, for example, in[27] for the fabrication of nanoporous silver ribbons from rapidly solidified Al-based $Al_{75}Ag_{25}$ alloy.

Antibacterial activity of AlOOH–Al composite nanoparticles

The results of time-kill studies of the synthesized nanoparticles against the tested pathogens are given in Fig. 7.

For the isolates of the Gram-negative *E. coli* bacteria incubated both with as-produced Ag–Al nanoparticles and with oxidized Ag–AlOOH nanocomposites, a significant decrease in bacterial viability was observed after only several hours. Ag–AlOOH nanocomposites possessed a significantly stronger antimicrobial effect (compared to Ag–Al nanoparticles) with total eradication of *E. coli* reached after 6 h of incubation, Fig. 6a. A similar albeit slightly slower bacterial killing trend was recorded for the Gram-positive MRSA bacteria. In control tubes, those with PBS only, the bacterial concentration after 6 hours of incubation remained at the same level as at the starting point. Similarly, practically no decrease in the colony count was observed in the test tubes with pristine AlOOH indicating that these nanostructures alone have no measurable antibacterial activity. This is quite in agreement with the lack of *E. coli* and *S. aureus* bacterial growth inhibition by plain AlOOH nanoparticles reported in.[28] Thus, the ability of Ag–AlOOH nanocomposites to rapidly kill bacteria must be due to the antimicrobial properties of Ag nanoparticles. At the same time, it has been previously reported that AlOOH (boehmite) nanosheets effectively adsorb *E. coli*, presumably due to electrostatic attraction of the negatively charged bacteria to the positively charged AlOOH surface.[29] It can be assumed that the mechanism of antibacterial effect of the Ag–AlOOH nanocomposites is realized by adsorption of microorganisms on AlOOH nanosheets and their subsequent inactivation by silver nanoparticles.

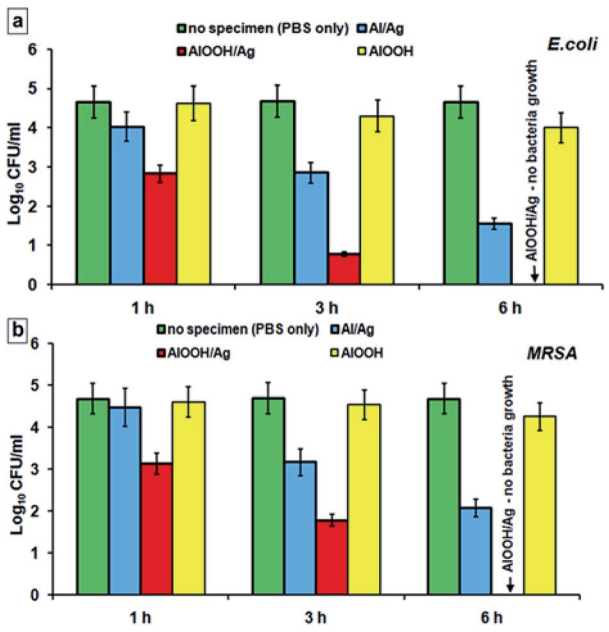

Fig. 7 Results of time-kill assay of AlOOH–Ag composite nanoparticles against *E. coli* (a) and MRSA (b).

Experimental

Synthesis of bimetallic nanoparticles

Bimetallic Ag–Al nanoparticles were produced by electric explosion of twisted wires in the atmosphere of argon at the pressure of 2 × 10^5 Pa. A detailed description of the electric explosion processing of bimetallic nanoparticles can be found in.[18] Silver wire with the diameter d = 0.15 mm and aluminum wire with the diameter d = 0.35 mm, both 80 mm long were used for electric explosion. The atomic ratio of Al-to-Ag in the wires was around 85 at% Al and 15 at% Ag. The capacitance of the capacitor bank (C) and the charging voltage (U) were 2.8 μF and 26 kV, respectively. The specific electrical energy input in each wire was approximately $2E_c$ (where E_c is the sublimation energy of the wire material). Ag–Al nanoparticles are pyrophoric immediately after synthesis. They are passivated by slow letting-to-air method before use. The surface of the particles is covered by a thin oxide layer.

Water oxidation of bimetallic nanoparticles

The reaction of bimetallic Ag–Al nanoparticles with water was conducted in a diluted water suspension. 1 g of the Ag–Al nanopowder suspended in 100 mL deionized water was placed in a thermally-insulated glass reactor equipped with combination pH electrode (ESK-10601) and temperature sensor (DTS-4-01). The suspension was heated from 23 to 67 °C at the heating rate of 1.0 °C min^{-1}, under continuous stirring. Since the oxidation reaction is exothermic and is accompanied by change in pH, the reaction progress was monitored by continuous recording of temperature and pH (with a Multitest IPL-103 pH-meter, Semico, Russia). To study intermediate oxidation products, the reaction was quenched by addition of isopropyl alcohol cooled to −23 °C and the sediment was filtered and dried at 120 °C for 2 h.

Characterization of bimetallic nanoparticles and their oxidation products

Phase identification was performed by X-ray diffraction (XRD), employing an XRD-6000 diffractometer (Shimadzu Corporation, Japan) with Cu-Kα radiation operating at 40 kV and 30 mA. The average crystallite size was determined from the broadening of the (111) XRD peak using the Sherrer equation. The lattice parameter was determined by the method of least squares. Microstructure characterization was performed using a JEM-

2100 transmission electron microscope, TEM (JEOL, Japan). Energy-dispersive X-ray (EDX) analysis and mapping was done using Oxford Instruments X-max detector (UK). TEM samples were by suspending the nanoparticles in ethyl alcohol and drying the suspension on a gold grid. The average nanoparticle size was determined by constructing particle size distribution histograms based on electron microscopy data. The resulting histograms of the particle size distribution were approximated using the normal-logarithmic law. Each histogram was constructed based on size measurements for 1281 particles. The minimum particle size was 18 nm, the maximum particle size was 311 nm. The average nanoparticle size d was 84 nm, the standard deviation was 0.379 and the coefficient of variation was 0.0045 (0.45%). A complete nitrogen adsorption isotherm was measured from relative pressures of 0.05 to 0.95 at 77 K on a Sorbtometer-M (Catakon, Russia) analyzer. The specific surface area was calculated by the BET method in the relative pressure range of 0.05–0.35. The zeta potential of nanoparticles was measured by their electrophoretic mobility (ZetaSizer Nano ZSP, Malvern Instruments, UK) at pH 7.4 and 37 °C in distillated water solution. 0.1 M NaOH were used to adjust the pH of the sample. Zeta potential is reported as the mean value of five independent measurements.

Antibacterial activity determination

The antimicrobial activity of Ag–Al nanoparticles and their oxidation products was tested by the viable counts method. In this method, *in vitro* killing dynamics of bacteria by the nanopowder was measured by counting the residual bacteria in comparison with the starter. Two bacterial strains were used in this study – *Escherichia coli* ATCC 25922 kindly provided by the Russian National Collection of Industrial Microorganisms, and the clinical strain of methicillin-resistant *Staphylococcus aureus* (MRSA) ATCC 43300 kindly provided by BioVitrum (Novosibirsk, Russia). For each strain, a bacterial suspension in PBS (phosphate buffered saline) with the concentration of 10^5 CFU mL^{-1} was prepared by dilution of the stock solution. 30 mg of the tested powder were added to 30 mL suspension contained in a sterile conical tube and incubated at room temperature under stirring on a magnetic stirrer PE-6600 (Ecroskhim, Russia). After 1, 3, 6, 9, 24 h, aliquots of 100 μL were collected from each test tube and diluted with sterile PBS. 30 μL of diluted suspension were spread on Müller-Hinton agar plates. The residual viable bacteria (CFU mL^{-1}) were counted after 24 h incubation at 37 °C. Micro-organisms in PBS only, and micro-organisms in the presence of boehmite nanopowder synthesized hydrothermally by reacting Al nanopowder with water[19] were used as controls.

For each sample, two independent experiments with five repetitions per sample per experiment were performed. Statistical analysis was performed by unpaired Student's t-test and $p < 0.05$ was considered statistically significant.

Conclusions

We created the facile one-step synthesis of AlOOH–Ag nanocomposite. The method described is straight-forward and environmentally friendly, the reaction takes place at low temperature (65 °C) and the sole starting reactants are Al–Ag nanoparticles and water, which favors the formation of contamination-free final products. Al–Ag nanoparticles prepared by electrical explosion of Al and Ag wires were used as a precursor. We've also demonstrated that the synthesized nanocomposites possess high antibacterial activity against both Gram-negative (*E. coli*) and high resistant Gram-positive (MRSA) microorganisms and can completely inhibit the growth of these pathogens. The bacterial killing capability of the AlOOH–Ag nanocomposites is believed to be due both to the presence of very fine antimicrobial Ag nanoparticles and to strong adsorption of bacteria by AlOOH. These results suggest that AlOOH–Ag is a promising antibacterial agent and that AlOOH is an attractive carrier of silver nanoparticles for biomedical applications. It should also be noted that the proposed approach can open new possibilities for production of metal-oxide nanocomposites using bimetallic nanoparticles of Al with another metal.

Conflicts of interest

There are no conflicts to declare.

Acknowledgements

The present work was financially supported by the Russian Science Foundation (Grant No. 17-79-20382). The antibacterial activity of AlOOH structures was financially supported by the Fundamental Research Program of the State Academies of Sciences for 2016–2020.

Notes and references

1 L. Ge, W. Wang, Z. Peng, F. Tan, X. Wang, J. Chen and X. Qiao, *Powder Techology*, 2018, **326**, 393.
2 Z. Yang, C. Qi, X. Zheng and J. Zheng, *J. Electroanal. Chem.*, 2015, **754**, 138.
3 S. Kulkarni, M. Jadhav, P. Raikar, D. A. Barretto, S. K. Vootla and U. S. Raikar, *New J. Chem.*, 2017, **41**, 9513.
4 A. A. Tsukanov and S. G. Psakhie, *Phys. Mesomech.*, 2017, **20**, 43.
5 H. Ni, Y. Guo, L. Wang, Y. Guo, W. Zhan and G. Lu, *Powder Technol.*, 2017, **315**, 22.
6 V. I. Mikhaylov, T. P. Maslennikova, V. L. Ugolkov and P. V. Krivoshapkin, *Adv. Powder Technol.*, 2016, **27**, 756.
7 C. Lei, M. Pi, W. Zhou, Y. Guo, F. Zhang and J. Qin, *Chem. Phys. Lett.*, 2017, **687**, 143.
8 X. Li, M. A. Shenashen, X. Wang, A. Ito, A. Taniguchi and S. A. Ei-Safty, *Sci. Rep.*, 2017, **7**, 16749.
9 D. Jana, A. Dandapat and G. De, *Langmuir*, 2010, **26**, 12177.
10 V. K. Sharma, R. A. Yngard and Y. Lin, *Adv. Colloid Interface Sci.*, 2009, **145**, 83.
11 Y. Y. Dong, S. Liu, Y. J. Liu, L. Y. Meng and M. G. Ma, *J. Mater. Sci.*, 2017, **52**, 8219.
12 B. L. Ouay and F. Stellacci, *Nano Today*, 2015, **10**, 339.

13 A. M. Jastrzębska, A. R. Kunicki, A. R. Olszyna and E. Karwowska, *Adv. Appl. Ceram.*, 2011, **110**, 108.
14 M. Chen, L. Yan, H. He, Q. Chang, Y. Yu and J. Qu, *J. Inorg. Biochem.*, 2007, **101**, 817.
15 Q. Chang, L. Yan, M. Chen, H. He and J. Qu, *Langmuir*, 2007, **23**, 11197.
16 N. V. Svarovskaya, A. V. Berenda, O. V. Bakina, E. A. Glazkova, A. S. Lozhkomoev, E. G. Khorobraya and A. N. Fomenko, *Prog. Nat. Sci.*, 2015, **25**, 1.
17 A. S. Lozhkomoev, E. A. Glazkova, N. V. Svarovskaya, O. V. Bakina, E. G. Khorobraya, S. S. Timofeev, V. V. Domashenko and S. G. Psakhie, *AIP Conf. Proc.*, 2014, **1623**, 367.
18 M. I. Lerner, A. V. Pervikov, E. A. Glazkova, N. V. Svarovskaya, A. S. Lozhkomoev and S. G. Psakhie, *Powder Technol.*, 2016, **288**, 371–378.
19 A. S. Lozhkomoev, E. A. Glazkova, O. V. Bakina, M. I. Lerner, I. Gotman, E. Y. Gutmanas, S. O. Kazantsev and S. G. Psakhie, *Nanotechnology*, 2016, **27**, 205603.
20 I. Yamauchi, T. Kajiwara, T. Mase and M. Saraoka, *J. Alloys Compd.*, 2002, **336**, 206.
21 V. A. Lubarda, *Mech. Mater.*, 2003, **35**, 53.
22 A. H. Geisler and J. K. Hill, *Acta Crystallogr.*, 1948, **1**, 238.
23 A. M. Emmanuelle, *Microsc. Microanal.*, 2007, **13**, 484.
24 A. V. Pervikov and M. I. Lerner, *Curr. Appl. Phys.*, 2017, **17**, 1494.
25 F. Yılmaz, D. J. Lee, J. W. Song, H. S. Hong, H. T. Son, J. S. Yoon and S. J. Hong, *Powder Technol.*, 2013, **235**, 1047.
26 Y. X. Zhang, Y. J. Z. Jin, X. Y. Yu, W. H. Xu, T. Luo, B. J. Zhu, J. H. Liu and X. J. Huang, *CrystEngComm*, 2012, **9**, 3005.
27 Z. Zhang, Y. Wang, Z. Qi, W. Zhang, J. Qin and J. Frenzel, *J. Phys. Chem. C*, 2009, **113**, 12629.
28 Z. Chen, D. Wu and J. Chen, *Appl. Phys. A: Mater. Sci. Process.*, 2015, **119**, 1515.
29 N. V. Svarovskaya, O. V. Bakina, E. A. Glazkova, A. N. Fomenko and M. I. Lerner, *Prog. Nat. Sci.*, 2017, **27**, 268.